PARALLEL BLADE-VORTEX INTERACTION ON PITCHING AIRFOIL

Andrea Colli*, Giuseppe Gibertini, Prajwal Urs Krishna, Veronica Marchesi, Alex Zanotti
Politecnico di Milano, Milano — Italy
* andrea.colli@polimi.it

Abstract
A wind tunnel test campaign was conducted to study the effects of parallel blade-vortex interaction on a retreating rotor blade, in particular in relation to the possible triggering of stall. A tandem configuration was succesfully used, with an upstream airfoil model which was impulsively pitched to generate a vortex, that subsequently interacted with a downstream NACA 23012 airfoil, representing the blade. Different conditions of angle of attack of the blade and relative trajectory of the vortex were studied. PIV measurements were taken to characterise the vortex and to investigate the flow on the suction side of the blade model during the BVI. The results show an effect of the vortex approach on a separated flow region in the case of high angle of attack of the blade. Preliminary test with the blade model oscillating have been performed, to simulate the pitching motion experienced by an actual rotor blade.

List of symbols

V_∞	wind tunnel free-stream velocity
d	vortex diameter
c	blade model chord
c_g	vortex generator chord
u	horizontal velocity component
α	blade model angle of attack
α_g	vortex generator angle of attack
ω	angular velocity
f	oscillation frequency
k	reduced frequency

1 INTRODUCTION

In recent years, research on blade-vortex interaction (BVI) has shown how this phenomenon can trigger the insurgence of dynamic stall on rotor blades and therefore have a relevant effect on the rotor performances [7] [1] [4] [2] . While earlier studies have focused on perpendicular BVI or oblique BVI, this work is investigating parallel blade-vortex interaction, i.e. an interaction in which the axis of the vortex lies parallel to the axis of the blade on which it impacts.

Given the intrinsic two-dimensional nature of parallel BVI, wind tunnel tests were performed on a stationary airfoil, representing the rotor blade, free to pitch around its quarter-chord axis; this approach had the advantage of a simpler setup with respect to a complete rotor model.

The study was focused on the flow environment encountered by the retreating blade of a rotor, characterised by a relatively low flow speed and higher angles of attack of the blade sections, features favouring the occurrence of stall.

Following a common procedure in literature [6] [5], the generation of the vortex was accomplished by impulsively pitching another airfoil, the vortex generator, placed upstream from the blade model. In particular, according to [6], a criterion for the production of a single, two-dimensional vortex is given by the requirement that the duration of the pitching motion is less than the time it takes for the air to travel one chord of the generator.

The test campaign included a preliminary vortex characterisation phase, followed by a series of measurements with the blade model fixed, at various angles of attack, and finally the tests with the model oscillating, in order to simulate the pitching motion of an helicopter rotor blade.

Particle Image Velocimetry was chosen to study the phenomenon because of the ability to measure the velocity field in the region around the airfoil and thus to easily identify the vortex and its effect on the flow.

2 WIND TUNNEL TEST SETUP

The experiment was conducted in the ”Sergio de Ponte” wind tunnel of Politecnico di Milano, a closed-circuit, closed-section wind tunnel, with a test section of 1.5 x 1 m, a maximum free stream speed of 55 m/s and a turbulence level less than 0.1%.

The test rig (Figure 1) was composed by two airfoil models: the vortex generator, a carbon-fiber composite model with a symmetrical airfoil section, chord c_g of 0.2 m and aperture 0.96 m, which was used to generate the vortex; and the blade model, an aluminum airfoil with a NACA 23102 section, a chord c of 0.3 m and an aperture of 0.96 m. The models were placed in the wind tunnel in a tandem configuration, with the vortex generator 3 chords upstream of the blade model. The vortex generator vertical position was manually adjustable via sliding the support braces along vertical struts, thus allowing to modify the vortex trajectory as needed.

47th European Rotorcraft Forum, Glasgow, 7-10 September, 2021

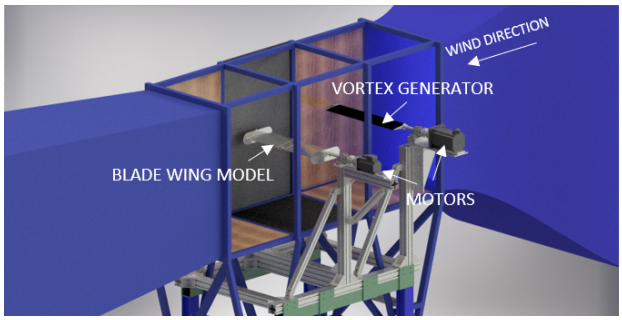

Figure 1: Schematics of the test rig.

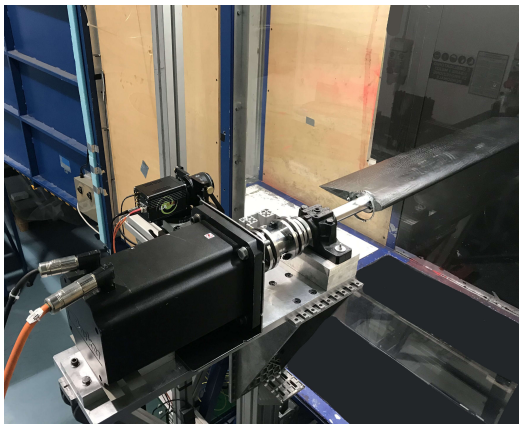

Figure 2: Test rig for the vortex generation measurements: the vortex generator is visible in the test section, with a PIV camera capturing the region immediately downstream. The flow is from right to left.

Each model was connected to a brushless electric motor, in order to be able to pitch it around the quarter-chord axis. For the airfoil model a Parker SME115 was chosen, with a nominal torque of 10 N m, while the vortex generator was powered by a Parker SME170, with a nominal torque of 35 N m and a peak torque of 110 N m; both motors were equipped with a Heidenhain SinCos EnDat encoder, with an accuracy of $\pm 400''$. The connection between motors and models was realised by means of a flexible joint coupling, equipped with self-aligning clamping elements, which allowed to compensate for any possible misalignment of the setup. In the following study any mechanical backslash or deformation of the models was neglected and their angular motion was assumed to be coincident with that of the motor shaft, so that the angular position of the airfoils was measured by the motors' encoders, after proper calibration.

The motors were operated by a programmable logic controller (PLC), which was programmed to iterate over a prescribed set of angular positions for each motor, generating a periodic motion with the desired shape and frequency and allowing to synchronize the motion of the two models.

In particular, for the vortex generator, since a fast pitching motion was required to generate a coherent vortex, a sawtooth wave was chosen, with an amplitude of 10 ° from $\alpha_g = -10°$ to $\alpha_g = 0°$. A series of tests was conducted by modifying the controller parameters and the input set of positions in order to reduce overshooting and oscillations on the actual motion of the system, while keeping the pitching motion as fast as possible. The final waveform included stationary intervals both before and after the impulsive pitching, and resulted in a sharp motion of 9.98 ° performed in 11.1 ± 0.1 ms.

Based on the characteristics of the obtainable motion, the wind tunnel free stream velocity was set at $V_\infty = 15\,\mathrm{m\,s^{-1}}$, corresponding to a chord-based Reynolds number of 300 000, which gave good results in terms of vortex formation; according to the criterion cited earlier, to this speed would correspond a pitching time threshold of 13.3 ms, which is larger than the one obtained.

For the PIV measurements a dual Nd-YAG Evergreen laser was used, with an energy of 200 mJ per pulse, together with two ILA sCMOS cameras, with a resolution of 2560x2160 pixel. The laser was placed below an optic window which was installed in the midspan of the test section floor. The image acquisition sequence was managed by a synchronizer which coordinated both the laser and the cameras; as trigger signal for the sequence, the output of a Hall effect sensor, installed on one end of the airfoil model, was employed, such that the signal would correspond to a predetermined angular position of the model (around $\alpha_g = 5°$). All the couple of images acquired were processed through the PivTec PivView2C software: correlation was performed with a multi-pass method over a 32x32 pixel grid and finally a phase average was computed from the resulting data.

3 TEST PROCEDURE AND RESULTS

3.1 Vortex generation and characterisation

In the first phase of the experiment the vortex generation was studied. The vortex generator was placed alone in the wind tunnel test section (Figure 2) and the PIV acquisition system was set in order to measure in a midspan longitudinal plane, including the trailing edge of the generator and the region immediately downstream.

For the following results, the generator reference frame is used, which is a cartesian reference frame with the origin taken coincident with the trailing edge of the vortex generator at 0 ° of angle of attack and the x direction aligned with the direction of the free stream.

A series of measurements were taken at four different time delays from the trigger signal, giving a separation between the measurements of 5 ms. For each of them, 200 couple of images were acquired.

As can be seen from Figure 3, by looking at the streamlines the vortex appears at first to form in a teardrop-like shape from the trailing edge of the generator airfoil. The core, considered as the region between the velocity components extrema, can be roughly described as an ellipse with a major axis of $0.225\,c_g$ and a minor axis of $0.12\,c_g$; the

circulation around the perimeter of the core was computed to be $0.53\,\mathrm{m^2\,s^{-1}}$.

At the following time instants, the shape of the vortex becomes more and more circular, while the streamlines in the outer region of the vortex show more irregularities.

In the last instant considered, some small secondary vortices can be seen trailing from the generator: their formation is probably due to small oscillations in the pitching motion of the airfoil, after the $10\,°$ rotation was completed. The controller parameters were adjusted to minimise these oscillations.

In all the images it is apparent the close relation of the generated vortex with the wake trailing from the airfoil: the vortex can be seen as an abrupt transition from the wake of the generator at the incidence of $\alpha_g = 0\,°$ to the wake at angle of incidence of $\alpha_g = -10\,°$.

In the last instant the vortex core has a circular shape with a diameter of $0.15\,c_g$ and its circulation was computed as $0.50\,\mathrm{m^2\,s^{-1}}$.

After these measurements on the generation of the vortex, the vortex generator was moved upstream, in the same position it would occupy in the tandem configuration, while PIV interrogation window was chosen centered approximately 4.5 c_g downstream of the generator's trailing edge, which is the position of the blade model leading edge in the tandem configuration. A series of measurements was performed to study the characteristics of the vortex in view of the later interaction experiments. Two sets of 200 couples of images were take, separated by a delay of 8 ms.

The results show that the vortex core has maintained its circular shape and has a slightly larger size, with a diameter of 31 mm. The circulation around the core perimeter is $0.36\,\mathrm{m^2\,s^{-1}}$, indicating that part of the vorticity has diffused outwards from the core.

The streamlines in the outer portion of the vortex still exhibit a more irregular shape; moreover, in the second set of images, the secondary vortices can be seen upstream of the main one.

The vortex centre positions, computed via the Γ_2 criterion[3], showed a very low dispersion, proving that the vortex generation had a good repeatability without meandering.

3.2 Static blade model

In the second phase of the study, the blade model was inserted downstream of the vortex generator (Figure 5) and its interaction with the vortex, generated as above, was investigated. PIV measurements were taken of the suction side of the airfoil at different times (Figure 6), allowing to study the evolution of the effects of the arrival of the vortex.

Two different vertical positions of the vortex generator were tested, named A and B, corresponding to different relative positions between the approaching vortex and the blade model. In particular, for the airfoil set at an angle of attack of $14\,°$, in case A the vortex centre was 52 mm above the leading edge of the blade model at a distance of 156 mm from it, while in case B the centre was 33 mm below the leading edge, when at a distance of 183 mm from the blade model. In the case of the airfoil set at an angle of attack of $10\,°$, only position A of the vortex generator was considered, with the vortex centre 54 mm above the leading edge, when at a distance of 157 mm.

For the following results, the blade reference frame is used, which is a cartesian reference frame with the origin taken coincident with the projection of the quarter-chord axis of the blade model and the x direction aligned with the direction of the free stream.

As can be seen from Figure 7, which represents the vortex arrival with the blade model at $\alpha = 10\,°$, the vortex at first is fully distinguishable by its streamline pattern, but as it approaches the blade model it becomes more difficult to visualize, as it is affected by the airfoil presence.

The effects of the interaction of the vortex on the flow on the suction side of the blade model can be seen in Figure 8 for the case of $\alpha = 10\,°$: while there is an evident alteration of the flow caused by the passage of the vortex, no particular effect arises in relation to flow separation, either at the leading edge or the trailing edge.

With the generator in position A, in Figure 9 the region upstream of the leading edge of the blade model at $\alpha = 14\,°$ is presented, showing the arrival of the vortex. While the vortex trajectory is slightly different from the previous case, due to the difference in the angle of attack of the airfoil, the behaviour of the vortex is similar.

The measures on the suction side, however, presented in Figure 10 (a) and (b), show a significant region of separated flow near the trailing edge of the airfoil; this region moves closer to the leading edge as the vortex passes over the airfoil (Figure 10 (b)).

To investigate in more detail the role of the vortex interaction, measurements were performed in the same configurations, but without pitching the vortex generator, which was kept fixed at $0\,°$ and $-10\,°$, to study the static influence between the two airfoils. As can be seen from Figure 10 (c) and (d), while with the vortex generator at $0\,°$ of angle of attack the flow on the blade model shows no separation, with the generator at $\alpha_g = 10\,°$ such a region can be seen near the trailing edge; this region, however, is less extended than the case with the vortex interaction. This behaviour can be explained by considering the fact that the airfoil is at a relatively high angle of attack and the effect of the incidence induced by the vortex generator at $10\,°$ can bring the blade to stall, while the same does not happen when the generator is kept at $0\,°$, given the much lower influence on the flow. The effect of the vortex is, apparently, that of aggravating the flow separation, especially when passing directly over the airfoil. It is expected that, once the vortex has been convected sufficiently far downstream, the flow would reattach and the situation would become that of Figure 10 (c).

Following these tests, the vortex generator was moved to position B, and new measures were conducted with the blade model at angle of attack of $14\,°$.

With the generator in this position the vortex approaches

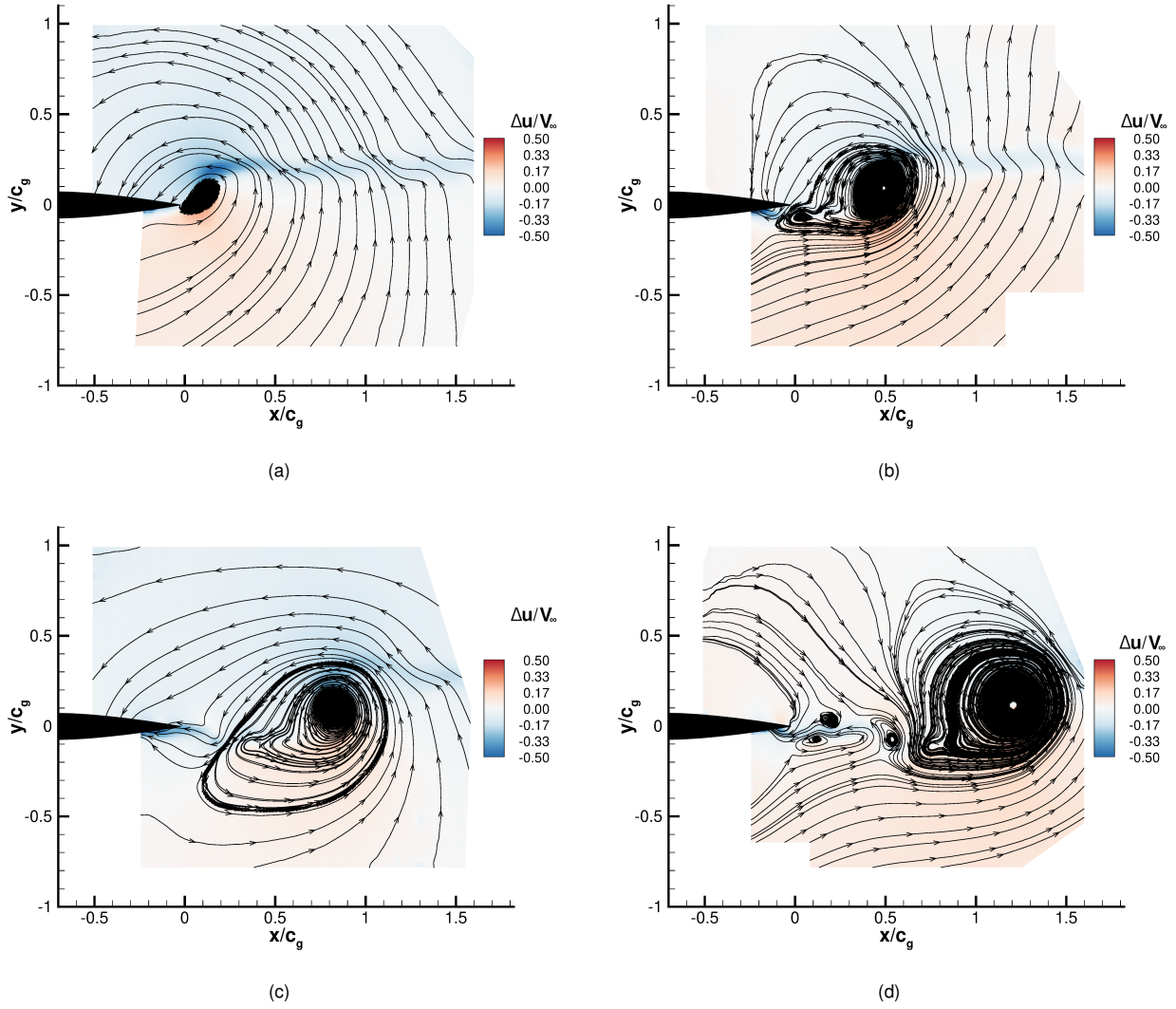

Figure 3: Phase averaged PIV measurements of the generation of the vortex after the impulsive pitching motion of the vortex generator. The images are separated by a time delay of 5 ms. The mean flow has been subtracted to visualise the vortex, contour thus indicates variations of horizontal component u of the velocity normalized with the free stream speed V_∞. The generator reference frame is used.

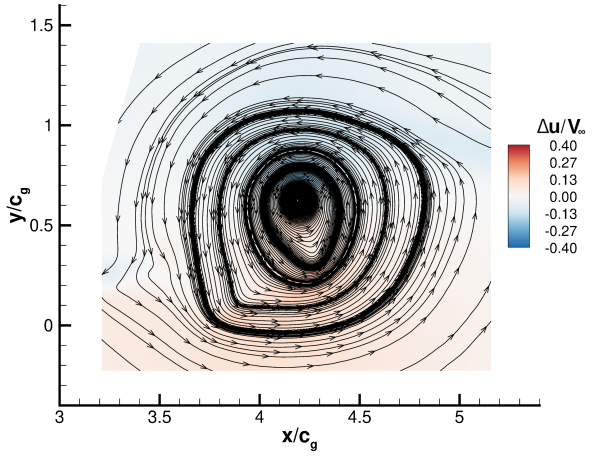

(a)

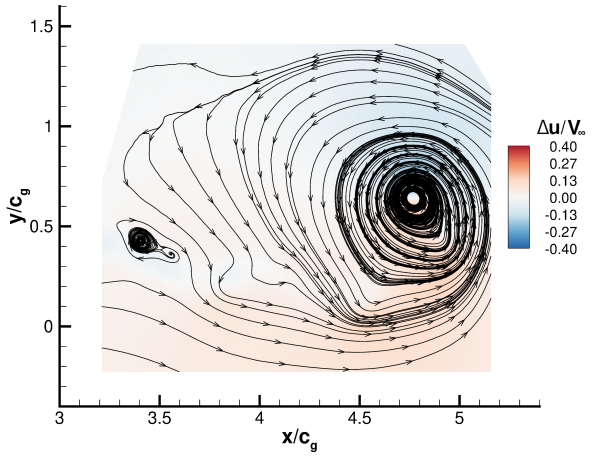

(b)

Figure 4: Phase averaged PIV measurements for the characterisation of the vortex after it was convected downstream. The images are separated by a time delay of 8 ms. The mean flow has been subtracted to visualise the vortex, contour thus indicates variations of horizontal component u of the velocity normalized with the free stream speed V_∞. The generator reference frame is used.

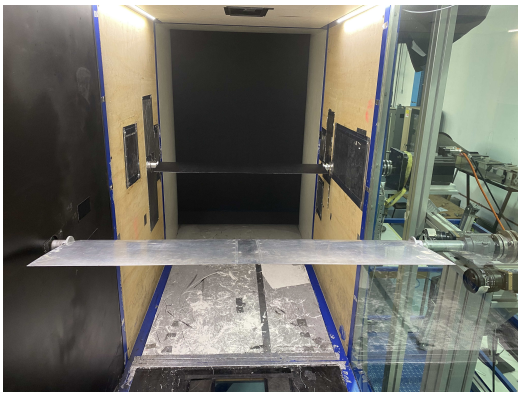

Figure 5: View from inside the wind tunnel of the test rig in the tandem configuration, with the vortex generator in the background and the blade model in the foreground. the flow is coming towards the reader.

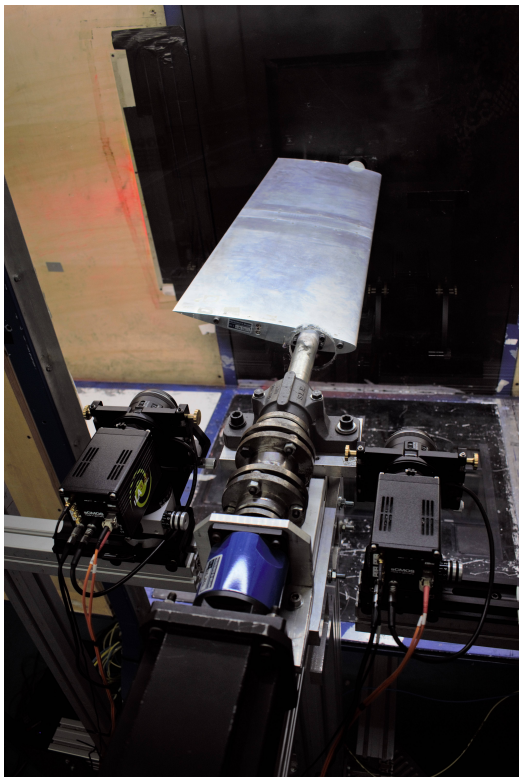

Figure 6: Detail of the setup for the measures on the suction side of the blade model. The flow is coming from right to left.

the airfoil from below the level of the leading edge, as can be seen from Figure 11, showing the arrival of the vortex for different time instants. The upward trajectory of the vortex can be followed from the deviation of the streamlines but, as in the previous cases, this effect is reduced as the vortex approaches the airfoil.

The effects of the vortex interaction on the suction side of the blade model are shown in Figure 12, including the interaction at four different time instants ((a)-(d)) and measurements with no vortex generation, but with the generator at $\alpha_g = 0°$ (e) and $\alpha_g = -10°$ (f), as was done in the previous case. From the results a region of flow separation is visible near the trailing edge of the airfoil, which is absent in the case of the generator fixed at $0°$ and again present with the generator at $-10°$. Differently from the previous measures, however, the effect of the vortex seems to be that of slightly reducing the separated flow region, while there is only a weak dependence on the time instants.

This difference in the behaviour of the interaction can be attributed to the different relative position of the vortex, passing over the suction side in the first case and approaching the airfoil from the pressure side in the second case. For the former, an explanation could be the following: given the counter-clockwise (in the airfoil reference frame) rotation of the vortex, its velocity field would tend to separate the boundary layer on the trailing edge of the airfoil; for the latter case, a similar explanation is not readily available.

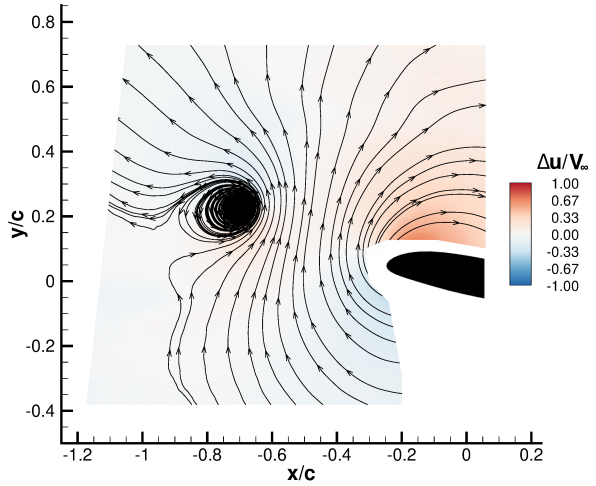

(a)

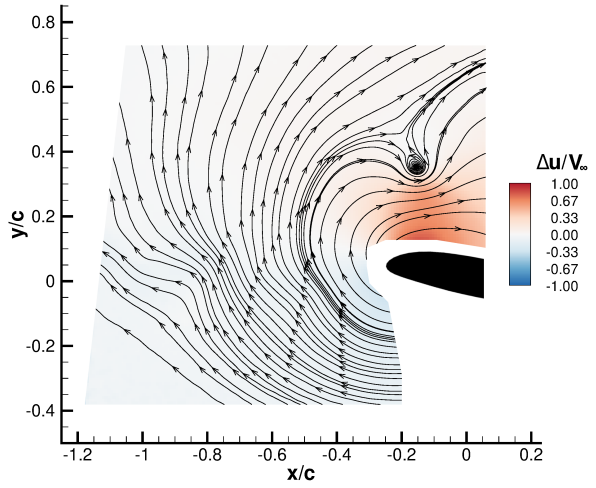

(b)

Figure 7: PIV measurements of the vortex interaction with the blade model at $\alpha = 10°$. The images are separated by a time delay of 10 ms. The mean flow has been subtracted to visualise the vortex, contour thus indicates variations of horizontal component u of the velocity normalized with the free stream speed V_∞. The blade reference frame is used. Measurements are phase averaged over 100 couples of images.

3.3 Pitching blade model

In the last phase of the study, the blade model was given an oscillating pitching motion to model the behaviour of an actual helicopter rotor blade and a series of measurements of the approach of the vortex was made, in order to provide results preliminary to the investigation of the possible triggering of dynamic stall of the blade.

The airfoil was pitched around an angle of attack of $\alpha_0 = 5°$ with an amplitude of $\Delta\alpha = 10°$, according to a sine law $\alpha = \alpha_0 + \Delta\alpha \sin(\omega t)$, with a reduced frequency $k = \pi f c / V_\infty = 0.1$ where c_a is the chord of the airfoil and f the frequency of the oscillation. The waveform of the vortex generator motion was adjusted accordingly.

The Hall effect sensor was moved to the blade model, so that the PIV system was triggered in to acquire a couple of images when the airfoil was at an angle of attack of 10°, representing the condition of a retreating blade. The vortex generator was in position B.

The results for the vortex arrival are shown in Figure 13 for two different time instants: the flowfield is markedly different from the previous static cases. The vortex trajectory, however, still has an upward path, with the vortex arriving from below the leading edge, as for the static case of Figure 11, and also the vortex appears to be less influenced by the interaction with the airfoil.

4 CONCLUSIONS

In this work a tandem setup with an impulsively pitching vortex generator has been successfully employed for the study of parallel blade-vortex interaction. The generation mechanism of the vortex has been investigated, showing how the vortex core, starting from an elliptical shape, acquires a circular shape after traveling about one generator chord downstream.

Subsequently, the interaction between the vortex so generated and the blade model, placed downstream, was investigated, for two different angles of attack of the blade and two different positions of the vortex generator. While for $\alpha = 10°$ no particular effect of the interaction was observed, for $\alpha = 14°$ the influence of the vortex could be seen on the trailing edge flow separation region, which was induced by the presence of the upstream vortex generator. In particular, when the vortex trajectory passed over the suction side of the airfoil, an adverse effect on the separation region was noticed, while an opposite effect could be seen with the vortex approaching from the pressure side.

While these phenomena were observed with the airfoil at a relatively high angle of attack, it is possible that the same mechanism could apply also to of lower angles of attack, in the case of stronger vortices, like those typically encountered in a rotor wake.

To further investigate this possibility, more tests could be performed with pressure measurements, allowing a better understanding of the effects of the flow separation.

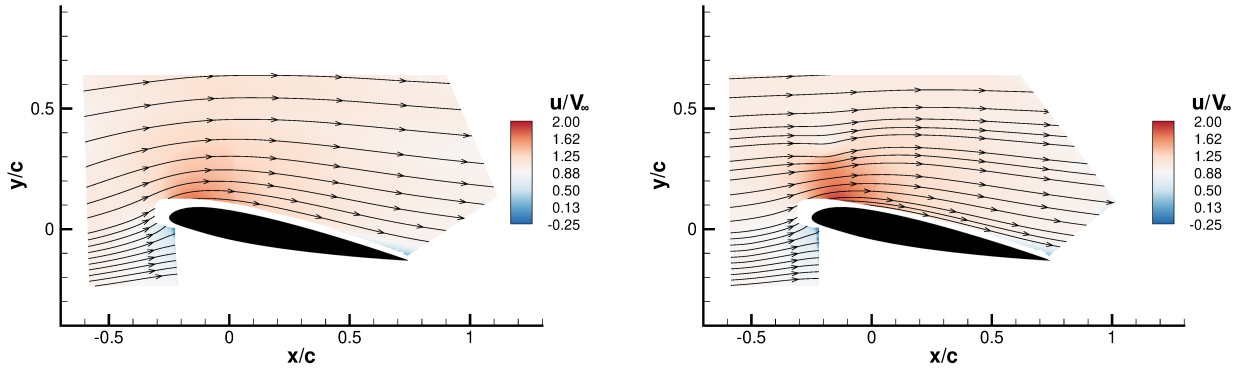

Figure 8: PIV measurements of the suction side of the blade model at during the interaction with vortex approaching the blade model at $\alpha = 10\,°$. The images are separated by a time delay of 10 ms and correspond to the same time instants as the respective images in Figure 7. Contour indicates the horizontal component u of the velocity normalized with the free stream speed V_∞. The blade reference frame is used. Measurements are phase averaged over 150 couples of images.

Finally, the preliminary dynamic tests showed the greater complexity of the flow with respect to the static case and a more thorough study is required.

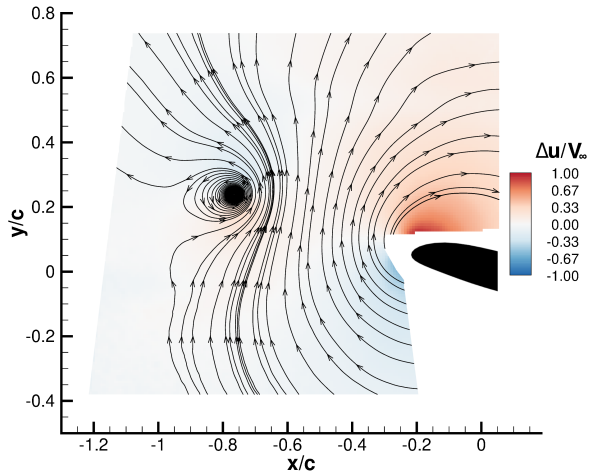

(a)

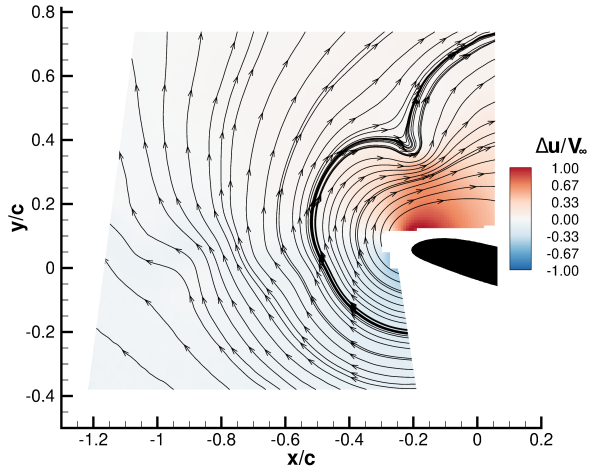

(b)

Figure 9: PIV measurements of the vortex interaction with the blade model at $\alpha = 14°$ and the vortex generator in position A. The images are separated by a time delay of 10 ms. The mean flow has been subtracted to visualise the vortex, contour thus indicates variations of horizontal component u of the velocity normalized with the free stream speed V_∞. The blade reference frame is used. Measurements are phase averaged over 100 couples of images.

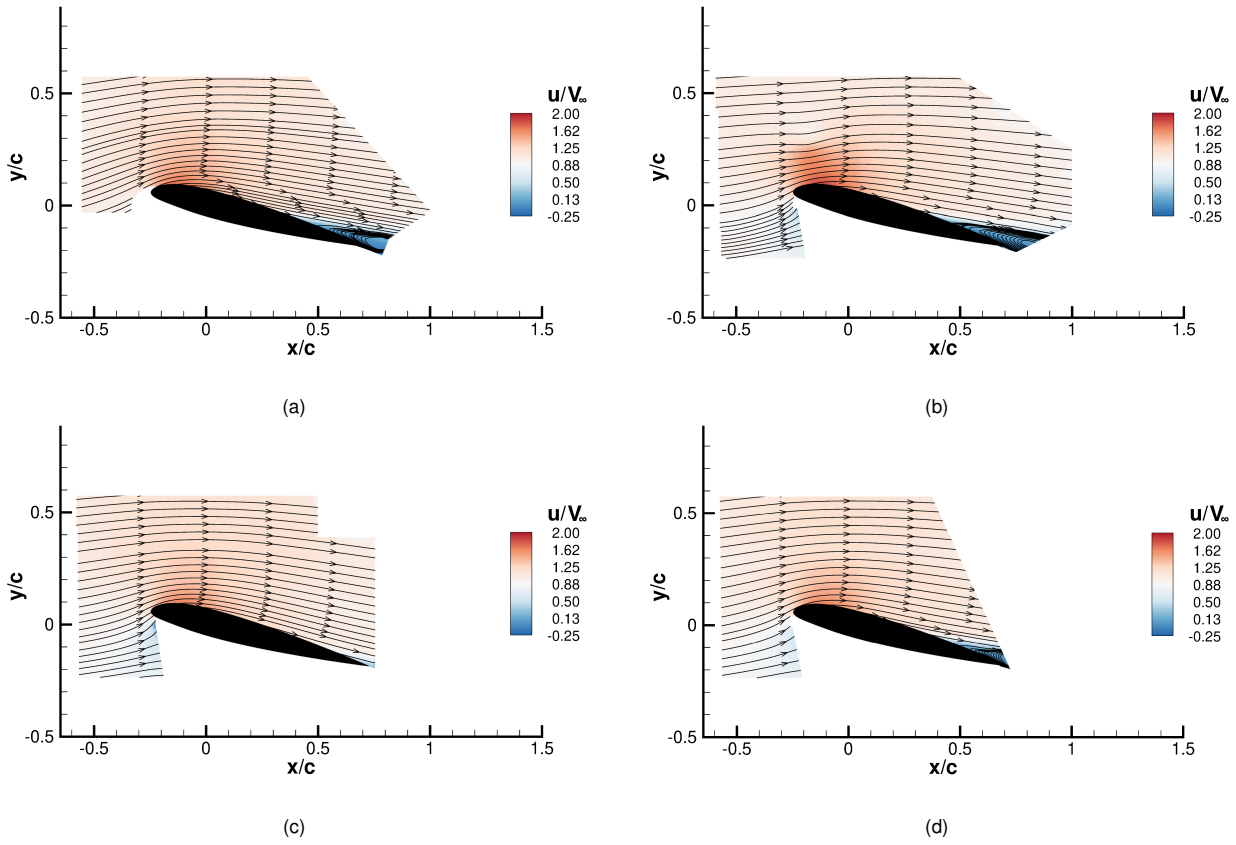

Figure 10: PIV measurements of the suction side of the blade model at during the interaction with the vortex ((a) and (b)) and with no vortex, with the generator fixed at 0 ° (c) and 10 ° (d). The blade model is at $\alpha = 14\,°$ and the generator is in position A. Images (a) and (b) are separated by a time delay of 10 ms and correspond to the same time instants as the respective images in Figure 9. Contour indicates the horizontal component u of the velocity normalized with the free stream speed V_∞. The blade reference frame is used. Measurements are phase averaged over 150 couples of images.

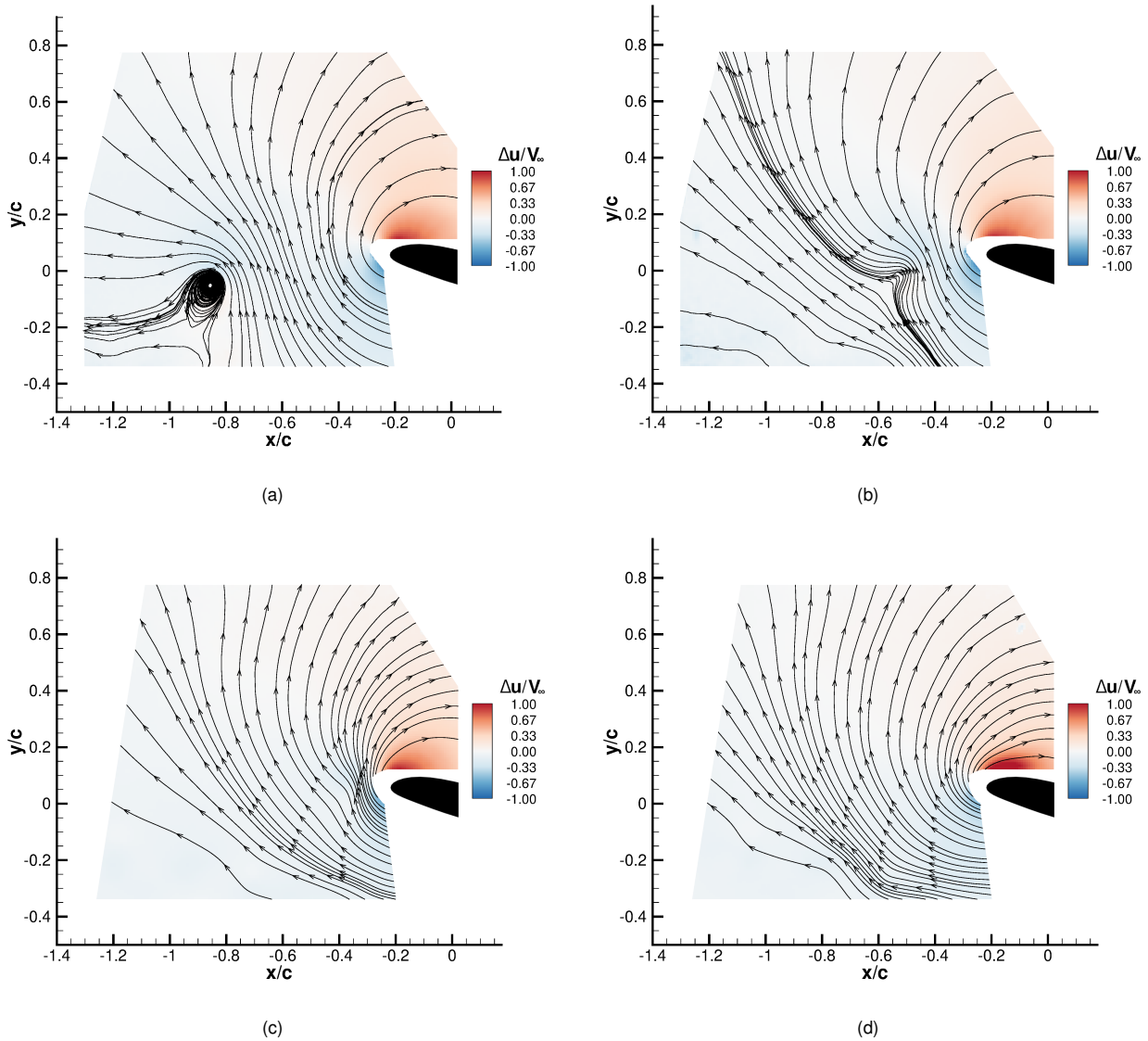

Figure 11: PIV measurements of the vortex interaction with the blade model at $\alpha = 14°$ and the vortex generator in position B. Image (a) and (b) are separated by a time delay of 8 ms, while (b), (c) and (d) are separated by a time delay of 3 ms. The mean flow has been subtracted to visualise the vortex, contour thus indicates variations of horizontal component u of the velocity normalized with the free stream speed V_∞. The blade reference frame is used. Measurements are phase averaged over 100 couples of images.

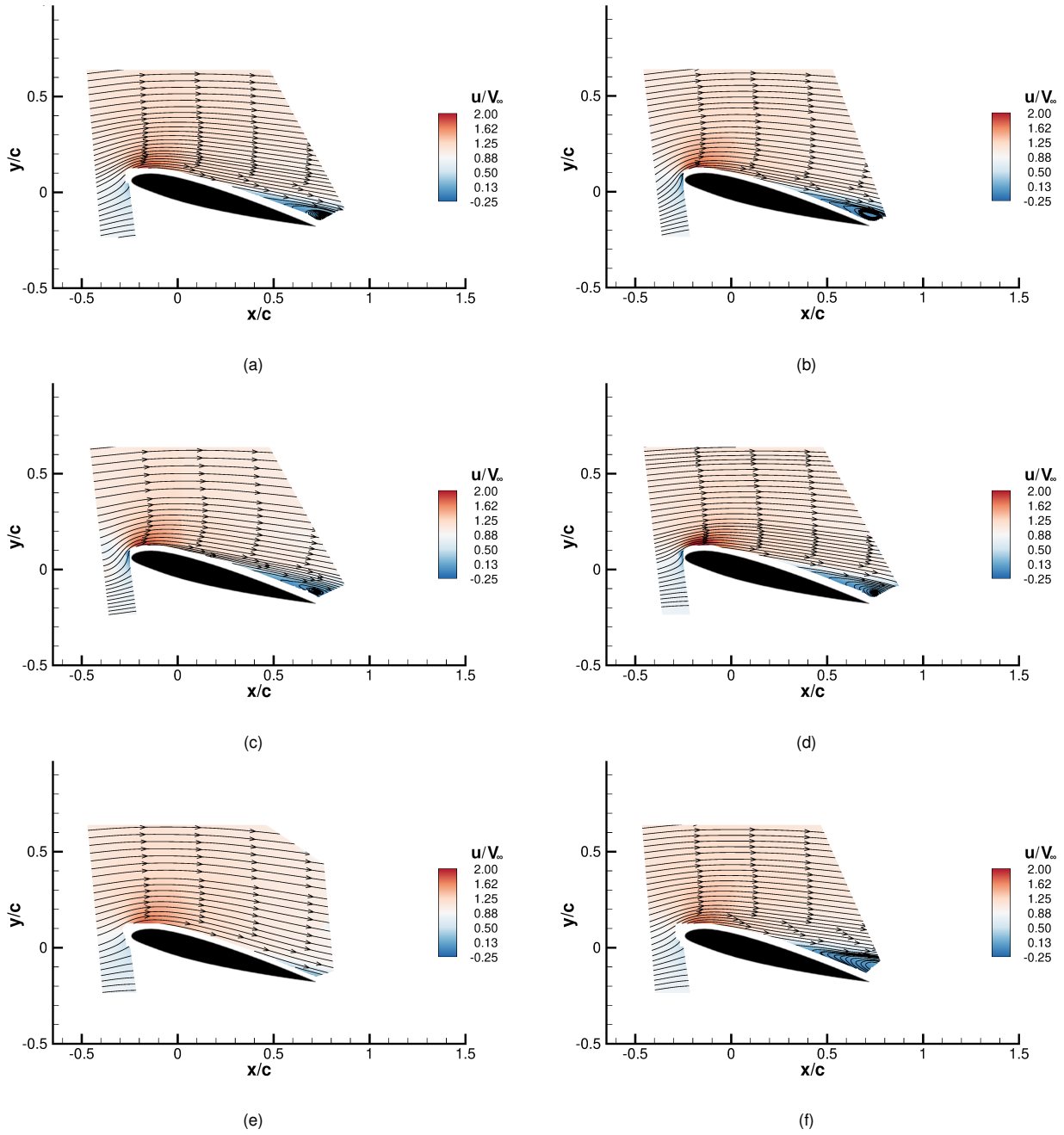

Figure 12: PIV measurements of the suction side of the blade model at during the interaction with the vortex ((a)-(d)) and with no vortex, with the generator fixed at 0° (e) and −10° (f). The blade model is at $\alpha = 14°$ and the generator is in position B. Images (a)-(d) correspond to the same time instants as the respective images in Figure 11. Contour indicates the horizontal component u of the velocity normalized with the free stream speed V_∞. The blade reference frame is used. Measurements are phase averaged over 150 couples of images.

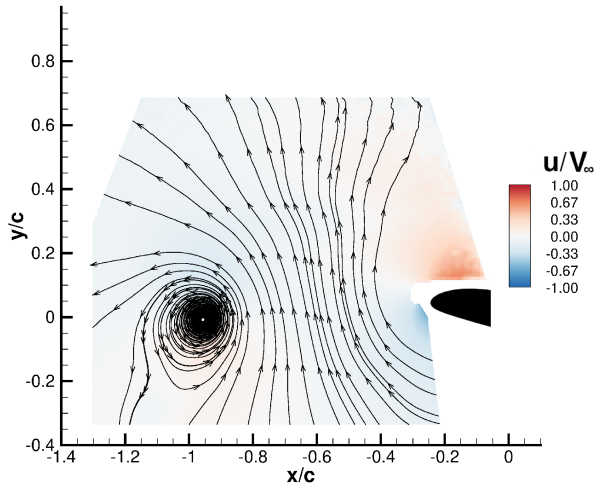

(a)

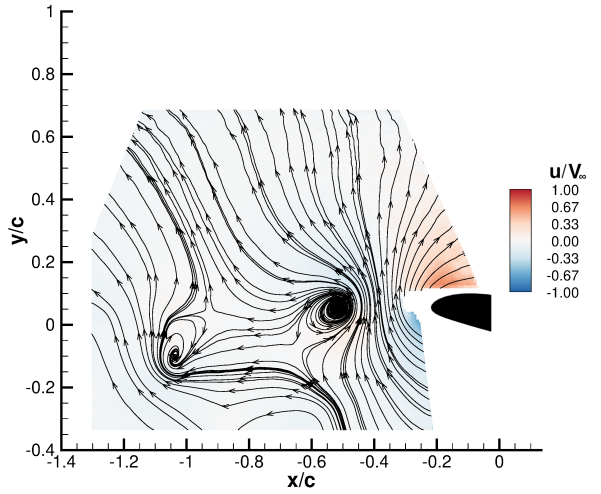

(b)

Figure 13: PIV measurements of the vortex interaction with the oscillating blade model at $\alpha = 10°$ and the vortex generator in position B. The images are separated by a time delay of 10 ms. The mean flow has been subtracted to visualise the vortex, contour thus indicates variations of horizontal component u of the velocity normalized with the free stream speed V_∞. The blade reference frame is used. Measurements are phase averaged over 100 couples of images.

Copyright Statement

References

[1] N. M. Chaderjian. Navier-stokes simulation of uh-60a rotorwake interaction using adaptive mesh refinement. In *Proceedings of the 73rd Annual Forum of the American Helicopter Society*, 2017.

[2] G. Gibertini, A. Colli, and A. Zanotti. Dynamic stall induced by blade vortex interaction in helicopter descending flight. *45th European Rotorcraft Forum (ERF 2019)*, 2019.

[3] M. Michard and T. Favelier. Développement d'un critère d'identification de structures tourbillonnaires adapté aux mesures de vitesse par piv. In *9ème Congrès Francophone de Vélocimétrie Laser*, pages 14–17, 2004.

[4] F. Richez. Analysis of dynamic stall mechanisms in helicopter rotor environment. *Journal of the American Helicopter Society*, 63(2):1–11, 2018.

[5] D. Seath, J.-M. Kim, and D. Wilson. Investigation of the parallel blade-vortex interaction at low speed. *Journal of aircraft*, 26(4):328–333, 1989.

[6] J. Straus, P. Renzoni, and R. Mayle. Airfoil pressure measurements during a blade vortex interaction and a comparison with theory. *AIAA journal*, 28(2):222–228, 1990.

[7] A. Zanotti, M. Ermacora, G. Campanardi, and G. Gibertini. Stereo particle image velocimetry measurements of perpendicular blade–vortex interaction over an oscillating airfoil. *Experiments in Fluids*, 55(9):1811, 2014.